



Reduced granitic magmas in an arc setting: The Catface porphyry Cu–Mo deposit of the Paleogene Cascade Arc

C.M. Smith ^a, D. Canil ^{a,*}, S.M. Rowins ^{a,b}, R. Friedman ^c

^a School of Earth and Ocean Sciences, University of Victoria, 3800 Finnerty Rd., Victoria, B.C., Canada, V8W 3P6

^b British Columbia Geological Survey, British Columbia Ministry of Energy and Mines, 1810 Blanshard Street, Victoria, B.C., Canada, V8W 9N3

^c Pacific Centre for Isotopic and Geochemical Research, Department of Earth and Ocean Sciences, The University of British Columbia, 6339 Stores Road, Vancouver, B.C., Canada, V6T 1Z4

ARTICLE INFO

Article history:

Received 19 April 2012

Accepted 1 August 2012

Available online 11 August 2012

Keywords:

Magma

Arc

Reduced

Oxygen fugacity

Apatite

Ore

ABSTRACT

The Catface porphyry Cu (Mo–Au) deposit, Vancouver Island, British Columbia was studied to characterize the age, geometry and geochemical affinity of its different intrusive phases, and their tectonic setting. Four different intrusive phases of quartz diorite are broadly calc-alkaline, moderately metaluminous, and have typical arc geochemical affinity. U–Pb age dating of zircons showing two intrusive phases was emplaced at 41.26 ± 0.11 and 41.15 ± 0.10 Ma, and a second two 40.93 ± 0.11 and 40.88 ± 0.10 (95% confidence). The latter ages are identical to the Re–Os age of molybdenite mineralization of 40.9 ± 0.2 Ma. The depth of emplacement is less than 4 km, as determined by amphibole–plagioclase thermobarometry (630–815 °C and 50–300 MPa). A reduced magmatic–hydrothermal system is evidenced by: (1) presence of pyrrhotite and absence of anhydrite and hematite, (2) low SO_3 (<450 ppm) in apatite, and (3) oxygen fugacities ($f\text{O}_2$) of 0.5–3.0 log units below the quartz–fayalite–magnetite (QFM) buffer recorded by the assemblage K-feldspar–biotite–ilmenite–quartz. Reduced porphyry-related magmas on Vancouver Island of similar age to those at North Fork, Washington (37 Ma) suggests consanguinity of reduced arc magmatism and related ore deposits within the Paleogene Cascade arc of the Pacific Northwest. Reduced evolved magmas at Catface are atypical in an arc setting, but can be attributed to thorough degassing of S from the magmas as evidenced by low S in apatite.

© 2012 Elsevier B.V. All rights reserved.

1. Introduction

Most porphyry Cu (Mo–Au) deposits throughout the world are associated with Mesozoic and Cenozoic orogenic belts (Sinclair, 2007). Porphyry deposits are defined as either classically oxidized or reduced on the basis of the mineralogy of the pluton, ore and associated alteration assemblages. The classic model involves ore fluids that are relatively oxidized, with $f\text{O}_2$ varying between the hematite–magnetite (HM) and nickel–nickel oxide (NNO) oxygen buffers at the temperatures associated with mineralization (Burnham and Ohmoto, 1980). Oxidized systems host significant amounts of primary magnetite, hematite, and sulfates, and are associated with oxidized I-type granitoids (Burnham and Ohmoto, 1980, 1981). In contrast, numerous porphyry Cu (Mo–Au) systems show strong evidence of having formed from relatively reduced ore fluids with $f\text{O}_2$ less than or equal to the QFM buffer (Rowins, 2000). These systems lack primary hematite and sulfate minerals, host abundant hypogene pyrrhotite, and can be associated with I-type, ilmenite-bearing granitoids as exemplified by the Paleogene North Fork Cu–Au deposit in the Cascades, Washington (Smithson, 2004).

The eastern margin of the Pacific Basin has extensive magmatism and associated porphyry-style mineralization during the Paleogene, in a semi-continuous belt from Oregon to Alaska (Fig. 1) (Madsen, 2004; Madsen et al., 2006). In this study, we investigate the age, geology, geochemistry and petrology of the intrusions on Vancouver Island hosting the Catface porphyry Cu (Mo–Au) deposit (Fig. 1) and place them within a regional context of Paleogene magmatism recognized on Vancouver Island (Madsen, 2004; Madsen et al., 2006). A combination of thermobarometry and oxybarometry is applied to quantify the oxidation states of the magmas, depths and temperatures of pluton emplacement. We highlight the presence of more “reduced” porphyry type magmas at Catface and their linkage to other similar examples in the Paleogene Cascade arc and highlight the conundrum of their occurrence in an arc setting.

2. Geological setting

Paleogene magmatism on Vancouver Island consists of plutonic and volcanic rocks emplaced into or on Mesozoic country rocks of the Wrangellia and Pacific Rim terranes (Fig. 2). The Catface deposit is situated at a northwest trending contact between mafic volcanic rocks of the Upper Triassic Karmutsen Formation and diorite and quartz monzonite of the Jurassic Westcoast Complex and Island Plutonic Suite

* Corresponding author. Tel.: +1 250 472 4180; fax: +1 250 721 6200.
E-mail address: dcanil@uvic.ca (D. Canil).

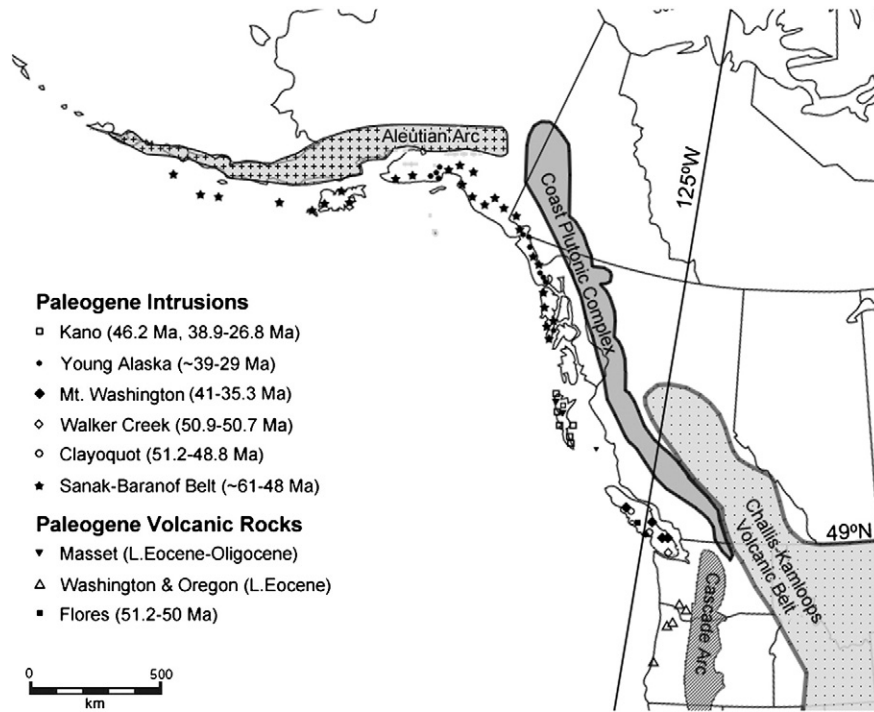


Fig. 1. Map showing of the Pacific Northwest showing locations of Paleogene forearc and arc magmatism (after Madsen et al., 2006).

(Fig. 3). Four intrusive phases are recognized (McDougall, 1976; McDougall and Enns, 1995): (1) a phaneritic quartz diorite at the center of the deposit (Catface phase), (2) porphyritic quartz diorite (Cliff and Halo Porphyry phases), (3) a phaneritic leucocratic quartz diorite southeast of the deposit (Hecate Bay phase), (4) hornblende-plagioclase porphyry (ADP) dykes. Regional faults strike northwest and northeast through the deposit (McDougall, 1976). Three distinct zones of mineralization have been recognized at the Catface porphyry deposit. The Cliff Zone (Fig. 3) hosts the bulk of the porphyry mineralization with an indicated resource of 56.9 million tons averaging 0.4% Cu and an additional inferred resource of 262.4 million tons grading 0.38% Cu

(Simpson and Chapman, 2009). Mineralization occurs as disseminated and fracture-controlled chalcopyrite, bornite, and molybdenite, with minor pyrrhotite mineralization in Triassic mafic volcanic rocks and in brecciated Jurassic quartz monzonite. In addition, lobes containing abundant magnetite, chalcopyrite, pyrite and pyrrhotite have also been identified.

Muller and Carson (1969) report a K–Ar age for the Hecate Bay quartz diorite of 48 ± 12 Ma. A pluton at Richie Bay, 4 km southeast of the Catface deposit on Meares Island, has a U–Pb zircon age of 41 ± 1 Ma (Isachsen, 1987). Madsen et al. (2006) identified two magmatic suites on Vancouver Island: the earlier Clayoquot (51.2–48.8 Ma) and the later

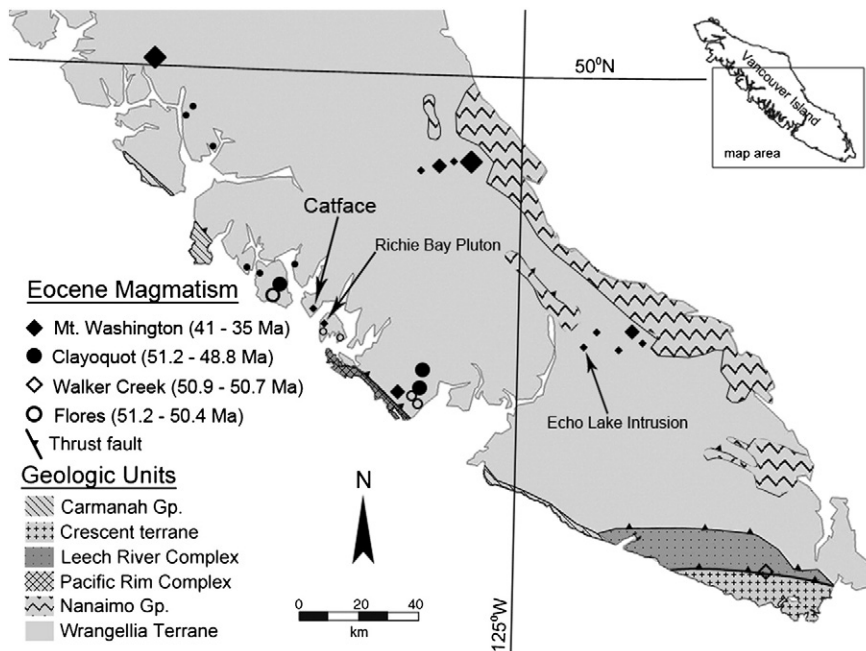


Fig. 2. Simplified regional geology of southern Vancouver Island showing locations of Paleogene intrusions, including that at of Catface and Echo Lake from this study (from Madsen, 2004).

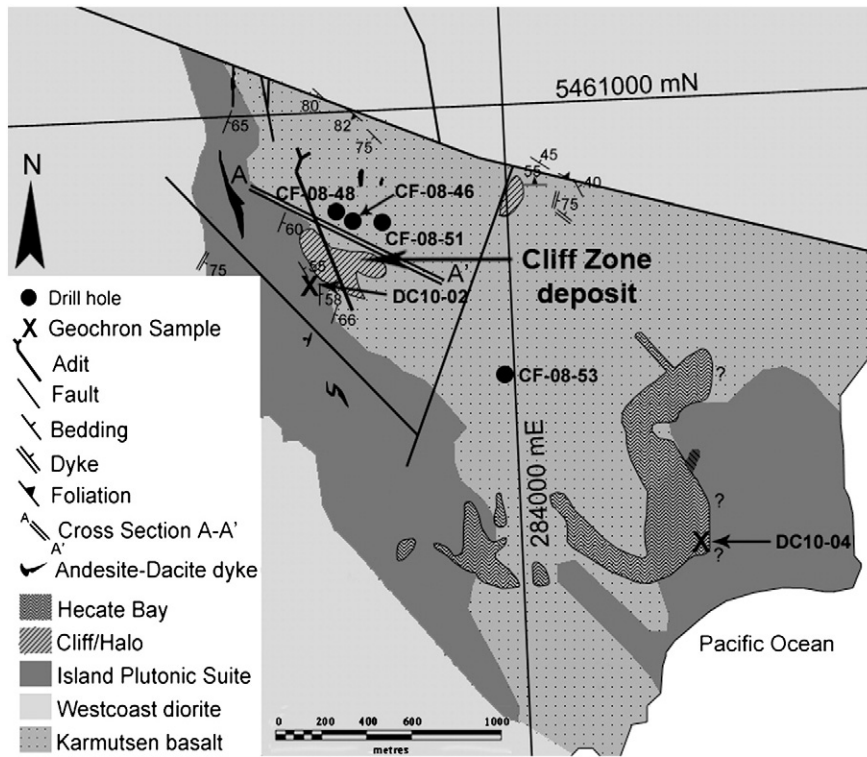


Fig. 3. Simplified geology of the Catface porphyry Cu–Mo deposit (modified after McDougall and Enns, 1995), with locations of drill holes (CF-08-48; CF-08-46; CF-08-51; CF-08-53) and outcrop samples used in this study. Also shown are cross-section A–A' (used in Fig. 4) and location of the Cliff ore zone.

Mt. Washington (41.0–35.3 Ma). The intrusions at the Catface deposit have not been dated using modern geochronologic methods and it is uncertain which if any of these suites they belong to.

A total of 1633 m of drillcore was logged from holes plunging 60 degrees southwest (orthogonal to the general strike of the deposit) allowing for the construction of a geological cross-section through the

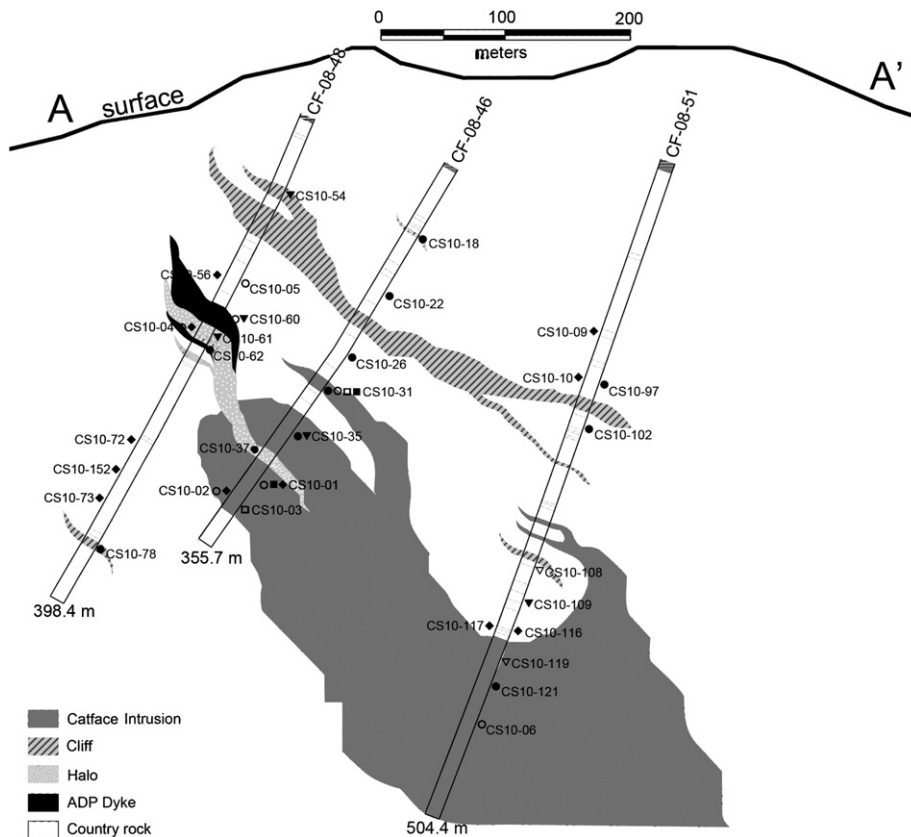


Fig. 4. Cross-section along A–A' (in Fig. 3) of the Cliff Zone viewed toward 030 azimuth, showing intrusive phases intersected in drillcore, and sample locations from this study.

deposit (Fig. 4). Over 160 core samples were collected, with additional sampling of outcrops along service and logging roads. A total of 20 samples were selected for detailed petrography, geochemistry and mineral chemistry (Fig. 4) and 9 for geochronology. In addition, samples from a Mt. Washington suite pluton east of Catface, with a U–Pb age of 37.4 Ma (Madsen et al., 2006) were also taken at Echo (Shelton) Lake for comparison (Fig. 2).

3. Analytical methods

U–Pb ages for zircons in all intrusive phases were determined at the University of British Columbia using methods described in Mundil et al. (2004) and Scoates and Friedman (2008). Isotopic dates are calculated using the decay constants $^{238}\text{U} = 1.55125\text{E}^{-10}$ and $^{235}\text{U} = 9.8485\text{E}^{-10}$ a^{-1} (Jaffey et al., 1971). Petrographic descriptions of each intrusive phase are given in Appendix A. Re–Os ages in molybdenite were determined by isotope dilution mass spectrometry at the University of Alberta using methods described by Selby and Creaser (2001) and Stein et al. (2007). Fresh samples with only primary igneous mineralogy were prepared for bulk rock geochemical analysis by cutting away any weathered or altered areas, crushed to 0.5 cm-sized fragments in a jaw crusher, and then powdered using an agate mill. Major and trace element abundances of 14 samples were determined at Acme Analytical Laboratories Ltd., Vancouver, British Columbia. Major elements were determined by XRF analysis. Trace element concentrations were determined by ICPMS on lithium metaborate and tetraborate fusion of 0.2 g samples followed by nitric acid digestion. Analytical accuracy and precision based on analyses of standards and duplicate samples are better than 10%. The major and minor element mineral compositions in eight samples (Supplementary Table 1) were determined at the University of British Columbia, using a Cameca SX-50 electron microprobe. Operating conditions were 15 kV accelerating voltage, a beam current of 20 nA for amphibole and ilmenite, and a beam current of 10 nA for feldspar, biotite, and apatite. Between 5 and 20 grains, including core and rims, were analyzed in each sample.

4. Geochronology

4.1. U–Pb zircon

Five of the seven U–Pb samples were from 1.5 m sections of drill core and the remaining two samples were gathered from outcrop. All interpreted ages and errors, except for the Halo phase, are based on weighted averages of $^{206}\text{Pb}/^{238}\text{U}$ dates for multiple concordant zircon analyses from each sample (Fig. 5, Table 1). Using weighted averages of $^{206}\text{Pb}/^{238}\text{U}$ data, the interpreted ages for the Cliff phase (CS10-54) are 41.15 ± 0.11 , slightly older (at 95% confidence) than the Hecate Bay (DC1004) and Catface (CS10-35) phases which have identical ages of 40.93 ± 0.11 and 40.89 ± 0.10 , respectively (Table 1). The Halo phase (CS10-61) produced a spread of ages between 41.4 and 40.4 Ma. The ADP dykes (CS10-60) crosscut all other lithologies and have youngest age of 40.71 ± 0.11 Ma. The U–Pb ages of all four phases at the Catface deposit are within error of those at Richie Bay on Meares Island, 4 km southeast, and fall in the age range of the Mt. Washington Intrusive Suite defined by Madsen et al. (2006).

Two samples (DC1002, CS10-109) described as Paleogene “Catface quartz monzonite” in previous work (McDougall, 1976; McDougall and Enns, 1995) produced unexpectedly older Jurassic ages and are now defined as pre-Paleogene wallrock of the Jurassic Island Plutonic Suite and thus unrelated to magmatism that formed the Catface deposit (Canil et al., in press; Isachsen, 1987).

4.2. Re–Os molybdenite

Molybdenite (MoS_2) is naturally enriched in ^{187}Re and contains insignificant nonradiogenic ^{188}Os (Selby and Creaser, 2001). As such,

essentially all ^{187}Os in molybdenite is derived from the decay of ^{187}Re . Several studies have proven the Re–Os in molybdenite system to be resistant to hydrothermal, or metamorphic resetting (Bingen and Stein, 2003; Raith and Stein, 2000; Selby and Creaser, 2001).

Molybdenite in two samples from the Catface deposit was dated using the Re–Os method. The Catface phase (CF10-119) hosts molybdenite as disseminated grains in a quartz–chalcopyrite–pyrite vein. The second sample (CS10-108) is from country rock of the Jurassic Island Plutonic Suite that hosts discrete blebs of molybdenite in a quartz–chalcopyrite–pyrite vein. The Re–Os ages for molybdenites in both samples were identical at 40.9 ± 0.20 Ma (Table 1) and within error of the U–Pb ages for the Catface or Hecate Bay phases at the deposit.

5. Geochemistry

All of the intrusive phases at Catface are quartz diorite (Fig. 6), are mostly metaluminous with Aluminum Saturation Indices (ASI—after Frost et al., 2001) ranging from 0.88 to 1.09 (Table 2), and plot within the calc-alkaline field on a FeO/MgO vs. SiO_2 diagram (Miyashiro, 1974). All Catface intrusive phases show trace element patterns typical of arc magmas with enrichments in Ba and Th and depletions in Nb and Ti (Fig. 7). There is considerable variation in K, Rb and Sr. On a Sr/Y versus Y diagram, only one sample (Cliff Porphyry—CS10-78) slightly overlaps the adakite field (Fig. 8).

6. Mineral chemistry

6.1. Amphibole

The majority of amphiboles in all intrusive phases at Catface deposit are magnesiohornblendes according to the classification of Leake et al. (1997). One sample from the Halo phase is Tschermakite enriched in Al, Mg and Na. Amphiboles have low Al_2O_3 from 3.5 to 5.4 (wt. %) in the Catface, Hecate Bay, and Cliff phases, whereas the Halo phase hosts Al-rich amphiboles with 8.9–11.5 wt. % Al_2O_3 . No significant intragrain compositional zonation in Fe# or Al was observed. Chlorine and to a lesser degree F contents correlate positively with Ti, Al, Na and K. The Echo Lake pluton has a very heterogeneous population of hornblendes, varying in Al_2O_3 from 5.9 to 12.6 wt. %.

6.2. Plagioclase

Plagioclase from the Catface phase varies in anorthite content (X_{An}) from An_{61-18} , often with rims enriched in An. The Cliff, Hecate Bay and Halo phases vary from An_{31} to An_{27} . Plagioclase in the Echo Lake pluton is notably sodic $\text{An}_{<10}$. Plagioclase showed extensive alteration to clay minerals in the ADP dykes and was not analyzed.

6.3. K-feldspar

Primary igneous K-feldspars in the Catface and Cliff phases are Or_{93-95} . No secondary K-feldspars (from mineralization) were recognized.

6.4. Biotite

The Hecate Bay and Catface phases have biotites with Fe# of 0.56, whereas the Cliff phase has slightly higher average Fe# of 0.63. Average abundances of TiO_2 in the Hecate Bay, Catface, and Cliff phases are all within 1 wt. % but a large range is observed in Catface of 0.85–4.96 wt. %.

6.5. Fe–Ti oxides

Ilmenites are hematite–ilmenite solid solutions and vary from $X_{\text{Hem}} (0.01-0.1)$, for the Catface phases and $X_{\text{Hem}} (0.04-0.09)$ for the Hecate Bay phase. Magnetites are nearly pure Fe_3O_4 with less than 2% ulvospinel (Fe_2TiO_4) component.

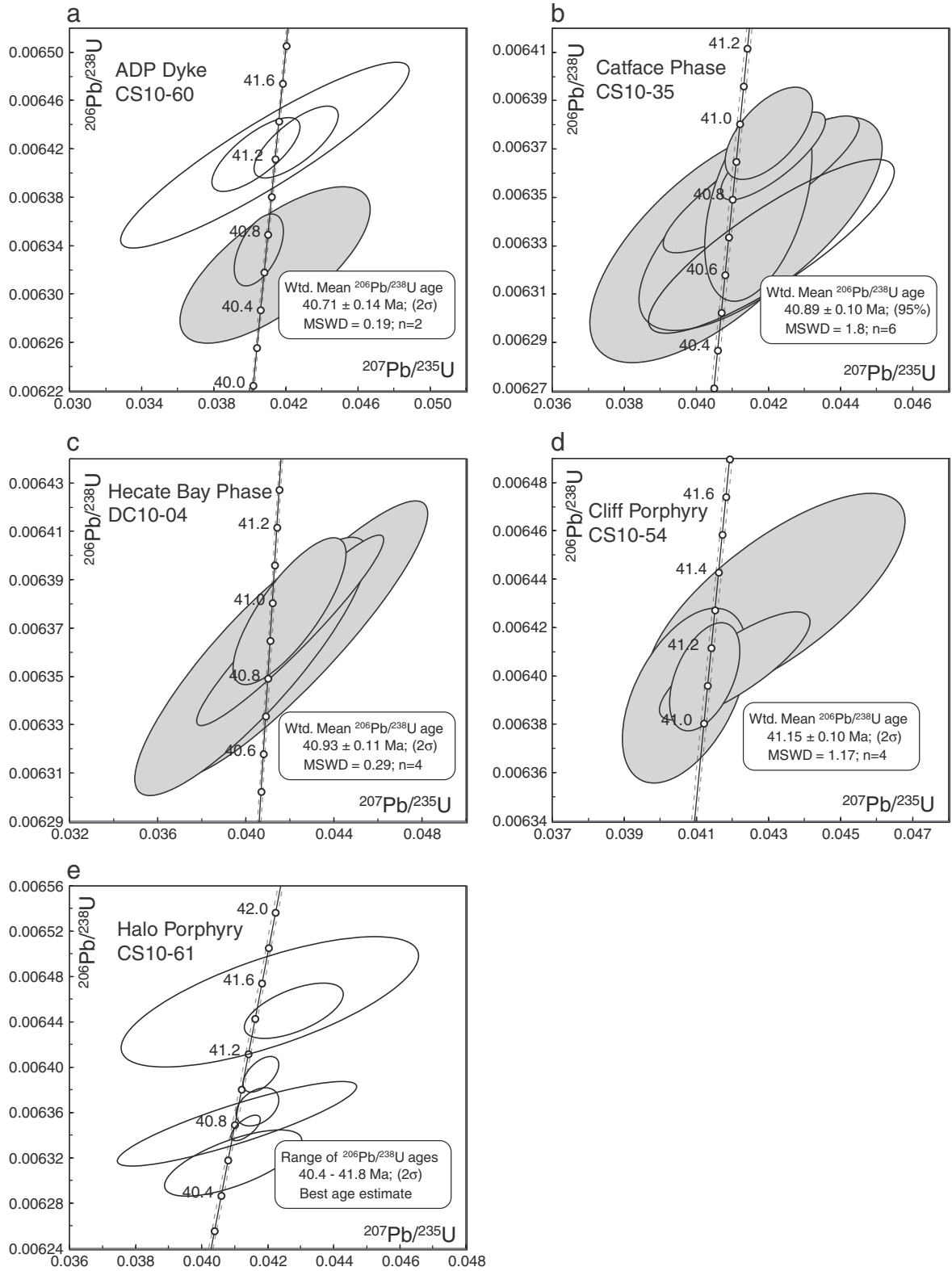


Fig. 5. U–Pb concordia diagrams for Catface porphyry deposit rocks, with errors plotted at 2σ . Shaded ellipses are used in calculation of weighted $^{206}\text{Pb}/^{238}\text{U}$ ages and unshaded ellipses not used. Concordia curve (solid line) is shown along with 2σ band, outlined by dashed lines.

6.6. Apatite

Analysis of three to ten apatite grains from four samples was intended as a monitor of the sulfate content of the magmas (e.g. Parat et al., 2002; Peng et al., 1997; Streck and Dilles, 1998). The SO_3 contents 40–200 μm in diameter grains in all phases at Catface

deposit are near or slightly above the detection limit (450 ppm). In all four samples analyzed, a slight decrease in Cl concentration is observed from cores to rims. All the Catface intrusive phases (Catface, ADP dykes, Hecate Bay) and the Echo Lake pluton contain very low SO_3 and Cl compared to data from other porphyry related intrusions in arcs (Fig. 9).

Table 1
Geochronology data.

Sample	Compositional parameters									Radiogenic isotope ratios							Isotopic ages						
	Wt.	U	Th	Pb	²⁰⁶ Pb*	Mol %	Pb*	Pb _c	²⁰⁶ Pb	²⁰⁸ Pb	²⁰⁷ Pb		²⁰⁷ Pb		²⁰⁶ Pb	Corr.	²⁰⁷ Pb		²⁰⁷ Pb		²⁰⁶ Pb		
	mg	ppm	U	ppm	× 10 ⁻¹³ mol	²⁰⁶ Pb*	Pb _c	(pg)	²⁰⁴ Pb	²⁰⁶ Pb	²⁰⁶ Pb	% err	²³⁵ U	% err	²³⁸ U	% err	coef.	²⁰⁶ Pb	±	²³⁵ U	±	²³⁸ U	±
(a)	(b)	(c)	(d)	(c)	(e)	(e)	(e)	(f)	(g)	(g)	(h)	(g)	(h)	(g)	(h)		(i)	(h)	(i)	(h)	(i)	(h)	
<i>CS10-60</i>																							
A	0.016	189	0.444	1.7	0.7964	89.06%	2.4	8.03	170	0.141	0.04637	2.60	0.0405	2.78	0.00634	0.38	0.523	17	62	40.3	1.1	40.72	0.16
B	0.016	45	0.371	0.6	0.1904	74.38%	0.8	5.39	72	0.118	0.04619	15.16	0.0409	16.05	0.00642	0.98	0.914	7	365	40.7	6.4	41.22	0.40
C	0.018	43	0.254	0.8	0.2046	65.34%	0.5	8.91	54	0.083	0.04747	9.85	0.0414	10.43	0.00632	0.83	0.712	73	234	41.2	4.2	40.64	0.34
F	0.004	109	0.471	0.9	0.1168	92.40%	3.6	0.79	243	0.148	0.04561	4.67	0.0403	4.95	0.00642	0.39	0.745	-23	113	40.2	1.9	41.23	0.16
G	0.003	175	0.492	1.6	0.1401	90.62%	2.9	1.19	197	0.162	0.04807	4.22	0.0426	4.49	0.00643	0.38	0.740	103	100	42.4	1.9	41.29	0.15
<i>CS10-35</i>																							
A	0.012	53	0.320	0.5	0.1691	88.75%	2.3	1.76	164	0.105	0.04780	6.22	0.0418	6.61	0.00634	0.57	0.708	89	147	41.6	2.7	40.74	0.23
B	0.004	141	0.572	1.2	0.1491	91.95%	3.5	1.07	230	0.183	0.04648	6.70	0.0406	7.11	0.00633	0.64	0.666	23	161	40.4	2.8	40.68	0.26
C	0.004	135	0.427	1.1	0.1425	93.90%	4.6	0.76	303	0.140	0.04766	2.72	0.0417	2.92	0.00635	0.53	0.449	82	65	41.5	1.2	40.79	0.22
D	0.005	139	0.367	1.0	0.1847	95.54%	6.3	0.71	415	0.120	0.04779	2.23	0.0420	2.36	0.00638	0.24	0.605	89	53	41.8	1.0	40.98	0.10
E	0.005	101	0.360	0.8	0.1332	93.99%	4.6	0.70	308	0.118	0.04799	2.65	0.0421	2.83	0.00637	0.23	0.797	99	63	41.9	1.2	40.92	0.09
G	0.011	95	0.374	1.1	0.2761	81.56%	1.3	5.13	101	0.124	0.04822	6.22	0.0421	6.62	0.00633	0.46	0.858	110	147	41.9	2.7	40.68	0.19
H	0.011	120	0.344	1.1	0.3484	87.26%	2.0	4.18	145	0.113	0.04770	5.00	0.0418	5.31	0.00636	0.36	0.868	85	118	41.6	2.2	40.84	0.15
<i>DC10-04</i>																							
B	0.020	42	0.545	0.5	0.2252	80.68%	1.3	4.43	96	0.179	0.04785	7.76	0.0420	8.24	0.00637	0.51	0.952	92	184	41.8	3.4	40.93	0.21
C	0.018	69	0.363	0.6	0.3316	88.62%	2.3	3.50	163	0.119	0.04776	4.71	0.0420	5.01	0.00638	0.39	0.780	87	112	41.8	2.1	40.98	0.16
D	0.013	43	0.511	0.6	0.1485	77.44%	1.0	3.56	82	0.169	0.04830	10.69	0.0424	11.35	0.00637	0.73	0.907	114	252	42.2	4.7	40.90	0.30
G	0.004	57	0.426	0.6	0.0599	84.07%	1.6	0.93	116	0.134	0.04592	10.12	0.0402	10.71	0.00635	0.69	0.871	-7	244	40.0	4.2	40.83	0.28
<i>CS10-54</i>																							
A	0.015	60	0.396	0.4	0.2389	96.07%	7.2	0.81	471	0.125	0.04615	3.28	0.0407	3.48	0.00639	0.46	0.493	6	79	40.5	1.4	41.07	0.19
B	0.030	51	0.378	0.4	0.4096	96.79%	8.8	1.12	576	0.121	0.04673	1.83	0.0412	1.95	0.00640	0.28	0.475	35	44	41.0	0.8	41.12	0.12
F	0.030	29	0.361	0.2	0.2296	92.07%	3.4	1.63	233	0.118	0.04763	3.83	0.0421	4.06	0.00640	0.29	0.813	81	91	41.8	1.7	41.15	0.12
G	0.010	56	0.465	0.5	0.1510	89.98%	2.7	1.39	185	0.155	0.04874	6.38	0.0432	6.77	0.00643	0.55	0.737	135	150	43.0	2.8	41.33	0.23
<i>CS10-61</i>																							
C	0.016	104	0.524	0.7	0.4399	98.90%	28	0.40	1685	0.171	0.047500	1.210	0.041686	1.272	0.006365	0.216	0.363	74	29	41.5	0.5	40.90	0.09
D	0.020	66	0.417	0.5	0.3524	98.05%	15	0.58	947	0.135	0.047408	0.975	0.041796	1.070	0.006394	0.203	0.542	70	23	41.6	0.4	41.09	0.08
E	0.019	77	0.513	0.5	0.3868	98.14%	16	0.60	995	0.166	0.047228	0.790	0.041329	0.878	0.006347	0.143	0.672	61	19	41.1	0.4	40.78	0.06
F	0.014	115	0.382	1.0	0.4228	90.44%	3	3.68	193	0.123	0.047037	3.890	0.040960	4.137	0.006316	0.378	0.681	51	93	40.8	1.7	40.59	0.15
G	0.010	151	0.398	1.2	0.4058	93.42%	4	2.35	281	0.131	0.048119	2.681	0.042793	2.854	0.006450	0.309	0.597	105	63	42.5	1.2	41.45	0.13
H	0.010	68	0.427	0.7	0.1784	84.63%	2	2.66	120	0.137	0.046904	6.795	0.041068	7.210	0.006350	0.477	0.878	44	162	40.9	2.9	40.81	0.19
J	0.004	86	0.676	1.0	0.0923	84.13%	2	1.43	117	0.219	0.047249	8.260	0.042072	8.759	0.006458	0.729	0.706	62	197	41.8	3.6	41.50	0.30

(a) A, B etc. are labels for fractions composed of single zircon grains or fragments; all fractions annealed and chemically abraded after Mattinson (2005) and Scoates and Friedman (2008).

(b) Nominal fraction weights estimated from photomicrographic grain dimensions, adjusted for partial dissolution during chemical abrasion.

(c) Nominal U and total Pb concentrations subject to uncertainty in photomicrographic estimation of weight and partial dissolution during chemical abrasion.

(d) Model Th/U ratio calculated from radiogenic ²⁰⁸Pb/²⁰⁶Pb ratio and ²⁰⁷Pb/²³⁵U age.

(e) Pb* and Pb_c represent radiogenic and common Pb, respectively; mol % ²⁰⁶Pb* with respect to radiogenic, blank and initial common Pb.

(f) Measured ratio corrected for spike and fractionation only. Mass discrimination of 0.23%/amu based on analysis of NBS-982; all Daly analyses.

(g) Corrected for fractionation, spike, and common Pb; up to 4.0 pg of common Pb was assumed to be procedural blank: ²⁰⁶Pb/²⁰⁴Pb = 18.50 ± 1.0%; ²⁰⁷Pb/²⁰⁴Pb = 15.50 ± 1.0%; ²⁰⁸Pb/²⁰⁴Pb = 38.40 ± 1.0% (all uncertainties 1-sigma). Excess over blank was assigned to initial common Pb with Stacey and Kramers (1975) model Pb composition at 41 Ma.

(h) Errors are 2-sigma, propagated using the algorithms of Schmitz and Schoene (2007) and Crowley et al. (2007).

(i) Calculations are based on the decay constants of Jaffey et al. (1971). ²⁰⁶Pb/²³⁸U and ²⁰⁷Pb/²⁰⁶Pb ages corrected for initial disequilibrium in ²³⁰Th/²³⁸U using Th/U [magma] = 3.

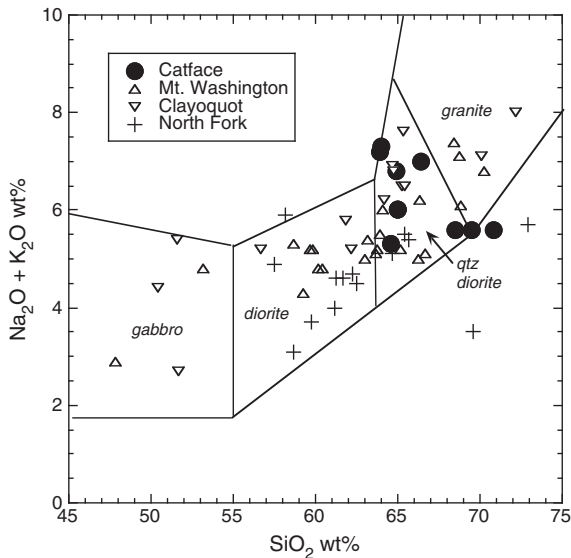


Fig. 6. Total alkalis versus silica plot for intrusive samples from the Catface deposit compared with those from North Fork, Echo Lake and other Vancouver Island intrusives (Madsen et al., 2006). Fields for rock classification are abbreviated from Middlemost (1994).

7. Thermobarometry and oxybarometry

Pressures and temperatures of emplacement of the Catface intrusions are calculated using the Al-in-hornblende geobarometer (Anderson, 1996; Anderson and Smith, 1995; Anderson et al., 2008; Hammarstrom and Zen, 1986; Schmidt, 1992), and the amphibole–plagioclase geothermometer (Holland and Blundy, 1994). Potential pitfalls of the Al-in-hornblende geobarometer include its dependence on plagioclase composition, temperature and oxygen fugacity. Anderson et al. (2008) recommend use of this geobarometer for samples which contain the required mineral assemblage (quartz–K-feldspar–plagioclase–biotite–hornblende–titanite–FeTi oxide) with plagioclase compositions in the range of $<An_{35}$, and hornblende with Fe# less than 0.65. These criteria were met for 6 of 20 samples examined from Catface (Supplementary Table 1).

The calculated pressures are 50–300 MPa (± 60) MPa, close to the lowest pressures of any experimental calibration for Al-in-hornblende barometry (Table 3) (e.g. Johnson and Rutherford, 1989; Schmidt, 1992). Estimated temperatures vary from 630 to 815 (± 40) °C and most samples plot just near or slightly below the water-saturated granodiorite solidus (Fig. 10).

All intrusive phases at Catface have accessory FeTi oxides but with a preponderance of ilmenite over magnetite (estimated petrographically to be in the ratio of ~9:1). The predominance of primary ilmenite over magnetite in granitoids is a qualitative indication of a relatively reduced oxidation state (Ague and Brimhall, 1988; Ishihara, 1977, 1981; Rowins, 2000). For a more quantitative estimate of oxidation state, the magnetite–ilmenite oxybarometer (Buddington and Lindsley, 1964) has proven problematic for plutonic rocks due to sub-solidus re-equilibration of magnetite during slow-cooling (Wones, 1989). On the other hand, ilmenite has been found to be resilient to changes in composition during cooling (Ague and Brimhall, 1988) and coupled with the annite (XFe) component in biotite, can be a monitor of fO_2 in granitoids (Wones and Eugster, 1964) by application of the K-feldspar–ilmenite–biotite–quartz assemblage a given temperature (T) at 300 MPa using the equation:

$$\log fO_2 = 2 \log a_{Hem} + 4/3 \log a_{Or} - 4/3 \log a_{Ann} - \log K + 4/3 \log a_{H_2O}$$

where $a_{Hem} = h \cdot X_{Hem}$ in ilmenite, $\log h = (1332/(T(K)) - 1.124)$, a_{H_2O} is assumed to be unity and pressure assumed to be 300 MPa (Ague and

Brimhall, 1988; Candela, 1989). The X_{Hem} of ilmenites was calculated using QUILF (Andersen et al., 1993) and an ideal mixing model assumed for a_{Ann} in biotite and a_{Or} in K-feldspar.

At 900 °C, the K-feldspar–ilmenite–biotite–quartz assemblage in the Catface and Hecate Bay phases records fO_2 of QFM-2, whereas the Cliff phase is more reduced at QFM-3.5. At the temperatures estimated from amphibole–plagioclase thermometry (630–815 °C) the fO_2 results are QFM-0.5 to QFM-1 (Fig. 11).

8. Discussion

8.1. Geology and emplacement of the Catface intrusions

A combination of drill core logging with new U–Pb zircon ages projected in section shows that the intrusions at Catface are not plug-like as in previous interpretations (McDougall and Enns, 1995) but rather were emplaced as 20–30 m thick sheet or sill-like bodies, dipping shallowly to the southeast (Fig. 4). The hitherto unrecognized “Catface” quartz diorite intrusion makes up the main mass of magma and is a sheet approximately 200 m thick, but is not exposed at the surface of the deposit. The relationship of the Hecate Bay phase to the other four phases in the center of the Catface deposit (Fig. 3) cannot be ascertained due to lack of drill hole information to the south, but it has an identical age to the Catface phase. The similarity in age and composition shows that all intrusions represent closely spaced events of limited volume. All other Paleogene intrusions on Vancouver Island are also small in volume and many have outcrop patterns consistent with tabular or sill-like geometries (c.f. Madsen et al., 2006).

Pressure–temperature conditions from amphibole–plagioclase thermometry for Catface intrusives are mostly near the wet-granodiorite solidus (Fig. 10) and indicative of a relatively shallow depth (<4 km) for emplacement. The P–T results are consistent with the presence of miarolitic cavities in the Halo phase, a feature generally restricted to epizonal conditions (Candela, 1997). The depths from Al-in-hornblende barometry should be considered maxima, due to the tendency of over-estimation of pressure using this barometer in granitoids crystallized below QFM (Anderson, 1996). While the fO_2 in Catface intrusions is lower than what is recommended for this barometer, the Fe# of amphibole is within the range recommended, and the results of <150 MPa are broadly consistent with textures and regional geology. For example, other Paleogene Mt. Washington Suite plutons on Vancouver Island are emplaced into Cretaceous sedimentary rocks of the Nanaimo Group (Madsen et al., 2006), which have a maximum thickness of 4 km (~ 130 MPa) (Mustard, 1994). In this regard, two samples produce pressures that are incompatible with the latter geological constraint, and may represent disequilibrium assemblages. The Halo phase has anomalously high Al in amphibole and a pressure >200 MPa, incompatible with the presence of miarolitic cavities. The Echo Lake intrusion has a heterogeneous amphibole population, and despite being sampled directly in contact with Nanaimo Group sedimentary rocks, produces a pressure of 300 MPa, far above that consistent with the maximum thickness of those country rocks.

8.2. Evidence for reduced magmas forming the Catface deposit

The Catface intrusions show evidence of having formed from a reduced magma. Primary ilmenite is far more abundant than magnetite, and the ore system also shows reduced mineral parageneses. Typical oxidized porphyries precipitate hypogene chalcopyrite, pyrite and bornite in equilibrium with primary hematite and anhydrite (Richards, 1990; Rowins, 2000; Seedorf et al., 2005; Sinclair, 2007; Streck and Dilles, 1998). Neither anhydrite nor hematite is present at Catface, and the abundant hypogene pyrrhotite is suggestive of a relatively reducing ore fluid. These characteristics of the ore system are in concert with fO_2 recorded by K-feldspar–ilmenite–biotite–quartz assemblages in the Catface, Hecate Bay and Cliff phases, which are orders of magnitude

Table 2
Whole rock geochemistry.

Sample	CS10-18	CS-10-18DUP	CS10-37	CS10-31	CS10-78	CS10-35	CS10-121	CS10-60	CS10-62	DC10-04	Echo Lake
Phase	Halo	Halo	Halo	Cliff	Cliff	Catface	Catface	ADP Dyke	ADP Dyke	Hecate Bay	Plag porphyry
Drill hole no. or UTM	CF-08-46	CF-08-46	CF-08-46	CF-08-46	CF-08-48	CF-08-46	CF-08-51	CF-08-48	CF-08-48	285,155 mE, 5,458,638 mN	405,346 mE, 5,441,554 mN
<i>Analyte (wt. %)</i>											
SiO ₂	63.9	64.0	66.4	70.8	64.9	68.5	69.5	64.6	65.0	67.7	65.0
TiO ₂	0.55	0.57	0.48	0.46	0.58	0.4	0.42	0.57	0.56	0.40	0.39
Al ₂ O ₃	15.68	15.75	15.86	14.28	16.2	14.84	14.8	15.35	15	15.77	17.19
Fe ₂ O ₃	5.53	5.44	2.25	2.44	3.24	3.96	3.77	5.47	4.91	3.81	3.55
MnO	0.05	0.05	0.04	0.04	0.04	0.03	0.04	0.05	0.03	0.04	0.06
MgO	2.23	2.26	1.66	0.97	2.25	1.28	1.35	2.32	2.06	1.65	1.98
CaO	2.82	2.83	4.28	3.84	4.71	3.6	3.56	3.77	3.69	4.16	4.35
Na ₂ O	3.82	3.86	5.24	4.78	4.92	3.6	3.85	2.98	2.84	4.25	5.00
K ₂ O	3.38	3.45	1.79	0.85	1.84	1.97	1.75	2.28	3.14	1.44	0.95
P ₂ O ₅	0.12	0.12	0.13	0.11	0.14	0.11	0.11	0.12	0.11	0.08	0.11
Ba	0.04	0.05	0.08	0.07	0.05	0.05	0.05	0.03	0.05	0.05	0.06
C	0.02	0.02	0.02	0.02	0.02	0.02	0.02	0.02	0.02	<0.02	0.03
S	0.02	0.03	0.05	0.05	-	0.22	0.09	0.4	0.57	<0.02	<0.02
Total	100.08	100.39	100.4	99.36	100.27	99.2	100.13	99.59	99.04	100.19	100.85
LOI	1.91	1.99	2.18	0.7	1.4	0.8	0.92	2.03	1.68	0.81	2.21
ASI	1.05	1.04	0.87	0.91	0.88	1.03	1.02	1.09	1.02	0.98	1.01
<i>Traces</i>											
V	88	91	55	42	73	49	47	85	78	58	49
Co	11.6	11.3	8.7	6.8	10.4	8.6	8.5	12.9	14.9	9.5	8.2
Ni	23	23.9	9.1	2.6	8.5	10.1	8.5	20.3	22	8.6	7.2
Cu	1216	1128	426	1773	272	2148	778	3933	5468	19	5
Zn	50	48	29	8	14	37	22	45	41	23	37
Ga	18	19	16	17	17	17	17	18	17	17	17
Rb	140	144	34	23	61	89	62	101	105	44	15
Sr	279	292	334	283	489	273	270	340	319	323	606
Ba	403	428	819	654	440	494	514	325	529	483	579
Y	10.6	10.5	12.2	15.6	11.4	11.5	13.7	11.2	9.3	11.5	5.8
Zr	115	127	110	204	118	173	161	112	114	97	71
Nb	8.2	7.2	7.2	10.8	9.6	9.8	9.7	6.9	6.6	7.3	3.7
Mo	2.3	1.1	2.3	16.6	0.7	3.5	10.4	0.6	4.3	0.8	0.7
Cs	2.4	2.3	2.7	0.9	2.1	2.8	2.4	4.6	3.2	1.7	1.1
La	19.6	16.2	15.6	28.4	15	25.5	23.6	14.3	14	12.5	8.9
Ce	36.2	30.2	30.1	49.3	29.5	46	43.7	28.9	27.5	25.6	18.4
Nd	15	13.8	13.7	17.6	13.4	16.4	16	12.4	12.4	11.8	9.2
Pr	4.2	3.5	3.5	5.2	3.5	4.9	4.6	3.4	3.2	3.1	2.2
Sm	2.5	2.8	2.4	3.0	2.5	2.7	2.8	2.5	2.2	2.5	1.8
Eu	0.82	0.85	0.77	0.92	0.97	0.88	0.85	0.79	0.63	0.62	0.67
Gd	2.3	2.2	2.4	2.8	2.4	2.3	2.5	2.4	2.0	2.2	1.4
Tb	0.38	0.36	0.39	0.48	0.39	0.39	0.43	0.38	0.32	0.37	0.20
Dy	2.0	2.0	2.1	2.9	2.1	2.0	2.3	2.1	1.5	2.1	1.1
Ho	<0.1	<0.1	<0.1	1	<0.1	<0.1	<0.1	<0.1	<0.1	<0.1	<0.1
Er	1.05	1.01	1.18	1.65	1.21	1.13	1.43	1.17	0.92	1.28	0.65
Tm	<0.1	<0.1	<0.1	<0.1	<0.1	<0.1	<0.1	<0.1	<0.1	<0.1	<0.1
Yb	1.03	0.99	1.17	1.63	1.12	1.09	1.43	1.03	0.93	1.15	0.55
Lu	<0.1	<0.1	<0.1	<0.1	<0.1	<0.1	<0.1	<0.1	<0.1	<0.1	<0.1
Hf	3.4	3.2	3.2	5.4	3.5	4.9	4.3	3.2	3.1	2.9	1.9
Ta	0.7	0.5	0.7	1.1	1.1	0.9	0.9	0.6	0.5	0.8	0.2
Pb	1.2	1.2	7.6	1.2	1.0	0.8	0.8	1.2	3.9	0.8	3.0
Th	3.8	3.4	3.7	6.4	3.8	5.4	5.8	3.1	3.2	3.8	1.3
U	1.1	1.2	1.2	2.1	1.4	1.7	2.0	1.1	1.2	1.4	0.4

lower than those typical of magmas associated with classic oxidized porphyry Cu deposits (Fig. 11).

In silicic calc-alkaline magmas, apatite crystallizes below 950 °C (Green and Watson, 1979) and is a record of the liquid line of descent. The sulfate (SO₃) contents in apatite in experiments on felsic liquids increase with *f*O₂ from <0.04 wt. % at the QFM buffer to >1.0 wt. % at the MH buffer (Peng et al., 1997). Furthermore, at the onset of anhydrite saturation in oxidized granitic magmas, compositional zoning in primary apatite crystals can show an abrupt decrease in SO₃ from core to rim (Parat et al., 2002; Peng et al., 1997; Streck and Dilles, 1998). Consequently, if the magmas at Catface were reduced during crystallization the apatites should yield low SO₃ concentrations, and exhibit no compositional zonation given an absence of primary anhydrite saturation.

When compared with apatites from classic oxidized porphyries in arcs (Imai, 2002, 2004), those from the Catface deposit have negligible SO₃, consistent with a magma below QFM (Fig. 9) and having barely any sulfate present during crystallization. The oxidation states estimated for the Catface magmas from apatite SO₃ concentrations (<NNO—Fig. 9) correspond well to those calculated from K-feldspar-ilmenite–biotite–quartz oxybarometry (Fig. 11). Higher levels of SO₃ in the apatites of oxidized porphyries (Imai, 2002) are consistent with oxidized magmatic systems (>NNO + 1). A caveat is that low S contents (as SO₃) in apatites can exist even in an oxidized magma if considerable S is lost or degassed, and not available to partition. Although we have no independent record of the S content in the original magma forming the Catface plutons, experiments under reducing conditions suggest at least 200 ppm S in silicic melts in equilibrium with fluid (Scaillet

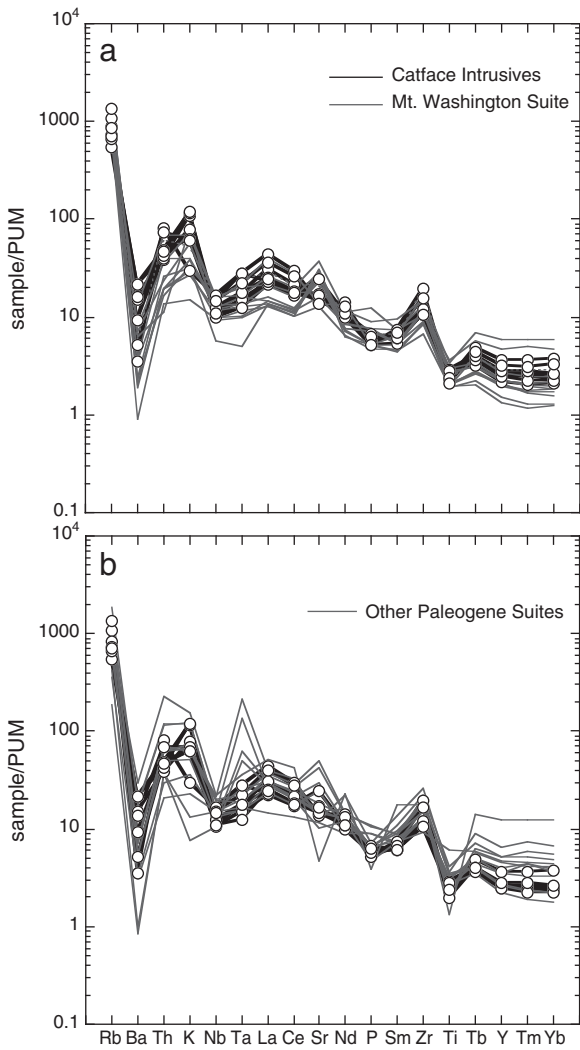


Fig. 7. Primitive upper mantle (PUM)–normalized trace element abundances of Catface intrusives (open circles) compared to (a) the Mt. Washington Suite intrusions (gray lines) from Vancouver Island (Madsen, 2004) and, (b) other Paleogene suites (gray lines) from Vancouver Island and North Fork, Washington (Madsen, 2004; Smithson, 2004). Trace element abundances for PUM from McDonough and Sun (1995).

and MacDonald, 2006; Zajacz et al., 2012). Assuming a K_D S apat/liq of 4.5 to 14 (Parat and Holtz, 2004), this would result in easily detectable S in apatite (>1000 ppm) even in a degassed magma.

8.3. Generation of reduced granitoid magmas in an arc setting

The age and trace element signature of all the intrusive phases at the Catface deposit (Catface, Cliff, Halo, ADP 0 Table 1, Fig. 7) show that they belong to the Mt Washington Suite (41–35 Ma) as defined by Madsen et al. (2006). Catface intrusions also have similar trace element patterns to the North Fork in the Cascades of Washington (Smithson, 2004) but with variable levels of Ba, Rb and Sr, attributed to differentiation. The similar geochemical affinity and ages of Catface, other Vancouver Island plutons, and North Fork, Washington (Fig. 7), and identical alteration and hypogene ore assemblages (pyrite–chalcopyrite–pyrrhotite), suggest the extension of reduced porphyry deposit magmas from the west-central Cascades of Washington to Vancouver Island.

Magmas in arcs are typically more oxidized than in other tectonic settings (Carmichael, 1991; Lee et al., 2005). Redox conditions for arc magmas range ~QFM-2 to QFM + 5 whereas OIBs and MORBs vary from ~QFM-2.5 to QFM. Several mechanisms can oxidize magma

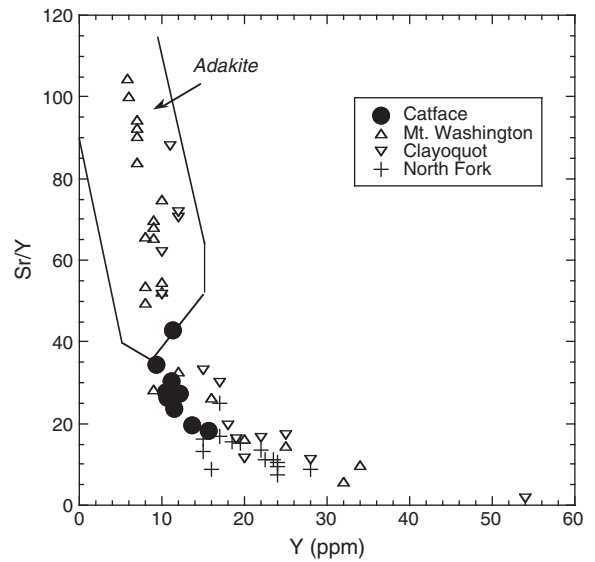


Fig. 8. Sr/Y–Y diagram showing Catface, North Fork, and other Paleogene igneous rocks from Vancouver Island (Madsen, 2004; Smithson, 2004) compared to the adakite field of Drummond and Defant (1990).

during its ascent (Ballhaus, 1993; Lee et al., 2005). If the source mantles for MORB or OIB all have a similar oxidation state (~FMQ—Lee et al., 2005) melts can become more oxidized when separated from that source due to the buffering of fO_2 by graphite–CO₂ (CCO) equilibria at the solidus changing to Fe³⁺–Fe²⁺ equilibria after graphite has been eliminated by partial melting (Ballhaus, 1993). Fractional crystallization during ascent or emplacement oxidizes magmas, as many liquidus minerals partition more ferrous than ferric iron (Carmichael, 1991; Mueller, 1971). Assimilation of oxidizing country rock or degassing of reduced volatile species (i.e. H₂, H₂S and CH₄) has also been proposed to increase oxidation state (Ballhaus, 1993; Holloway, 2004; Lee et al., 2005; Mathez, 1984).

Few mechanisms generate reduced magmas, especially in arc settings. Reduced calc-alkaline magmas at Catface are thus somewhat

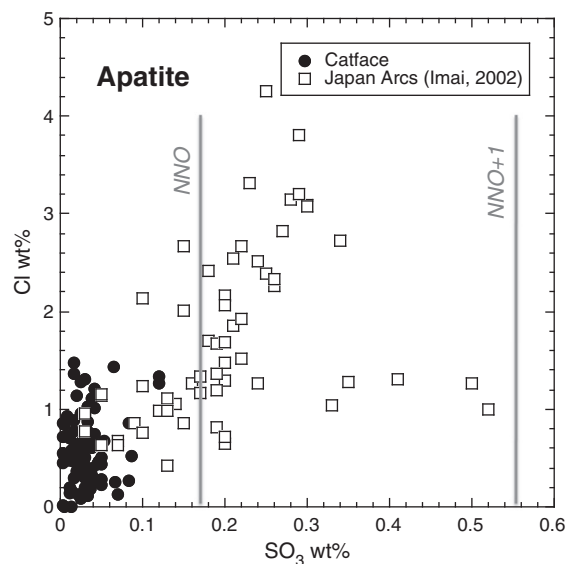


Fig. 9. Covariation of SO₃ and Cl for apatites from Paleogene Catface and the Echo Lake pluton on Vancouver Island, compared to a compilation for several porphyry related intrusives in the Japan arc (Imai, 2002). Vertical lines are the minimum SO₃ levels observed for apatites in silicic liquids equilibrated at various fO_2 given in log units relative to the NNO buffer (after Peng et al., 1997).

Table 3
Thermobarometry and oxybarometry.

Intrusion (sample)	Temp (C) ^a	±	P (Mpa) ^b	±	log fO ₂ (at 900 C) ^c	±
Catface (cs1003, cs1001)	662	12	186	24	-14.5	0.6
Catface (cs1006)	687	39	55	84		
Halo (cs1004)	808	10	285	16		
Cliff (cs1031)	639	12	80	37	-15.7	0.3
Hecate (dc1004)	684	35	114	13	-14.3	0.2
Echo Lake	743	6	296	246		

^a hbl-pl thermometry (Holland and Blundy, 1994).

^b Al-in-hornblende barometry (Anderson and Smith, 1995).

^c Ksp-Biot-Qz-Ilm equilibria (Ague and Brimhall, 1988).

of a conundrum if formed in an arc. One possibility is that the Paleogene magmatism in the Pacific Northwest resulted from the subduction of a mid-ocean ridge and formation of a slab window (Madsen et al., 2006). The slab window setting could impart a pulse of lower-*f*O₂ MORB-like mantle into the overriding mantle wedge, thereby having a source region at a lower *f*O₂ than typical of arc magmas. Nevertheless, the geochemistry of plutonic rocks at Catface clearly has an arc signature, and shows no geochemical evidence of derivation from a MORB or OIB-like mantle source.

In the Peninsular Ranges of California, Gastil et al. (1990) distinguished linear eastern magnetite-bearing and western ilmenite-bearing plutonic subprovinces, interpreted to have formed by a variable depth of magma generation along a subducting plate. There is no evidence of a linear belt of Paleogene reduced, ilmenite-series granitic rocks paired with oxidized magnetite in the Paleogene Cascades.

The subduction of C- and S-rich sediments could lead to the production of reduced arc magmas and ilmenite-series plutonism (Takagi, 2004). Upon dehydration of the down-going plate and supracrustal material, C from ocean floor sediments reacts with H₂O to produce CH₄ and CO₂ (Ballhaus, 1993; Takagi, 2004). In the Japanese arc, Takagi (2004) shows that S isotope compositions of magnetite-series granitoids are typically heavier than those of the ilmenite-series, and that this distinction reflects different sources of S because there is only minor isotopic fractionation of S at magmatic temperatures (Ohmoto and Goldhaber, 1997). Magnetite-series granitoids derive their S mainly from seawater

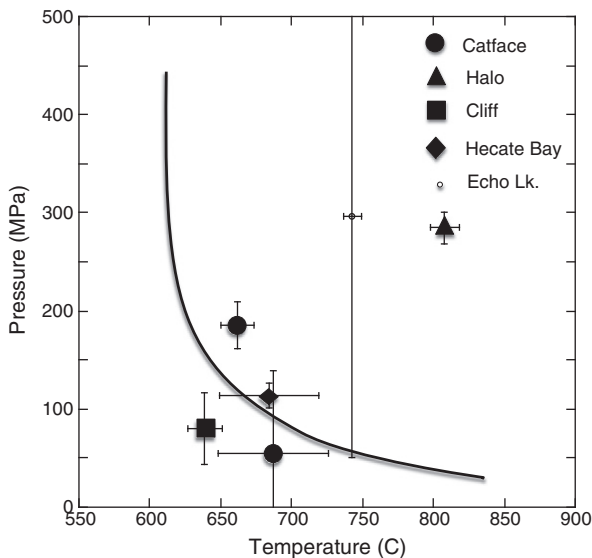


Fig. 10. Pressures and temperatures for different intrusive phases at Catface and the Echo Lake pluton estimated from Al-in-hornblende barometry and amphibole-plagioclase thermometry, compared to the water-saturated granodiorite solidus (line) (after Piwinski, 1968; Schmidt and Thompson, 1996). The wide uncertainty of pressure calculated for the Echo Lake pluton is due to extensive heterogeneity in Al content of its amphiboles. Uncertainties in pressures and temperatures are plotted at 1σ.

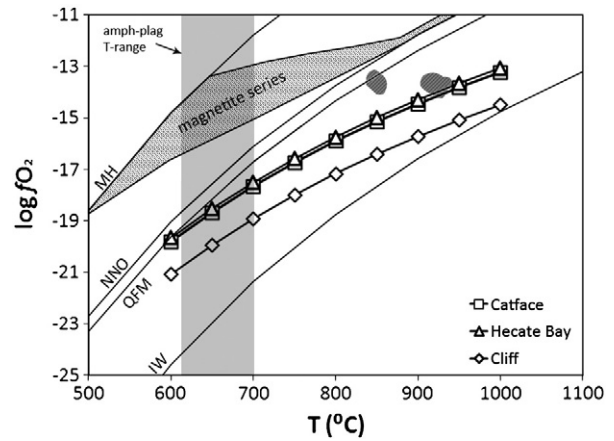


Fig. 11. Temperature-*f*O₂ estimates at 300 MPa recorded by the assemblage K-feldspar-biotite-ilmenite-quartz using the method of Ague and Brimhall (1988) for the Catface, Cliff and Hecate Bay intrusive phases, compared to those of 'magnetite series' granitoids (Burnham and Ohmoto, 1980; Ishihara, 1977) and two magmatic phases of the Paleogene North Fork deposit, Washington, USA (gray hatched fields—Smithson, 2004). Vertical shaded bar encompasses the range of temperatures from amphibole-plagioclase thermometry from this study. Buffer abbreviations: MH (magnetite-hematite); NNO (nickel-nickel oxide); IW (iron-wustite).

(as oxidized sulfate) whereas ilmenite-series magmas derive S mainly from reduced sulfide in metasedimentary rocks (Takagi, 2004). Significant input of reducing sedimentary material to a subduction zone could fundamentally reduce arc magmas at their source. We have no S isotope evidence available to test this model at Catface. Nevertheless, the ⁸⁷Sr/⁸⁶Sr ratios for Paleogene intrusives on Vancouver Island are all juvenile (<0.704) (Andrew et al., 1991; Isachsen, 1987), and much lower than in the study Takagi (0.705–0.709), indicating no significant sediment signature.

Alternatively, parental Catface magmas may have acquired a low *f*O₂ during their ascent through the crust. On Vancouver Island, the Pacific Rim Terrane lies structurally below Wrangellia and contains a considerable section of graphitic metasediments (Brandon, 1989; Fairchild and Cowan, 1982). Paleogene Catface magmas may have ascended through and interacted with this potentially reducing country rock. The low Sr⁸⁷/Sr⁸⁶ ratios (<0.704) of the Catface intrusives compared to the metasediments of the Pacific Rim terrane of (0.706–0.708) suggest little if any contamination to change Sr isotopes. Nevertheless, interaction with graphitic metasediments remains a viable mechanism as only 1 mole of C is required to reduce 4 moles of ferric iron according to:



Interestingly, the Catface intrusions have *f*O₂ nearly identical to the C—CO—CO₂ buffer at similar pressure-temperature conditions.

The introduction of H₂O via slab dehydration to a mantle wedge composed of olivine and orthopyroxene can generate significant quantities of serpentine. If temperatures remain less than 700 °C, and sufficient water and time are available, serpentinization of the entire forearc mantle wedge is possible (Hyndman and Peacock, 2003). Given the high *f*H₂ of fluids yielded by serpentinization (Barnes et al., 1978), and the reducing nature of phases that form within serpentinites, this rock has a high capacity to reduce magmas with which it interacts (Frost and Beard, 2007; Moody, 1976). Indeed one of the curiosities of Paleogene magmatism on Vancouver Island is that it was located far toward the trench/forearc (Madsen et al., 2006), at least in present-day coordinates. Interaction of Paleogene mantle-derived magmas with an overlying serpentine-bearing forearc mantle could potentially lower magmatic *f*O₂ (Frost, 1985; Frost and Beard, 2007) but this scenario would require the locus of magma production far toward the fore-arc region, where temperatures are typically too low to cause magma production above the subducting plate. Thus, although a number of

scenarios are possible to produce reduced magmas by interaction with wall rock, none of these can adequately explain the present isotopic or geochemical data for the Catface intrusions.

The more compelling argument for reduction of magmas involves sulfur (Anderson and Wright, 1972) an important volatile constituent of almost all arc magmas. The 8-electron change in redox state from S^{2-} to S^{6+} state, and degassing as SO_2 (S^{4+}) has significant reduction capacity. Using ferric iron contents and S in melt inclusions, Kelley and Cottrell (2012) document how fractional crystallization coupled with degassing of S in a subvolcanic arc magma chamber can result in significant reduction of magmas ($>2 \log fO_2$ units) varying from basaltic andesite to dacite. Their model fits well with mineral chemical evidence from the Catface intrusions. Using the partition coefficients of S between apatite and rhyolitic melt of Parat and Holtz (2004) (K_D S apat/liq = 4.5 to 14) the S contents of magmas in equilibrium with apatites from Catface are calculated to be less than 100 ppm, as observed (Fig. 9). These levels are at the low end of other degassed intermediate to felsic magmas (75–870 ppm—Scaillet et al., 1998) but similar to that predicted by partitioning of S between fluid and a reduced melt (Zajacz et al., 2012). The low apatite SO_3 contents of Catface apatites suggest not only reducing conditions, but also magmas that have lost considerable S, likely the cause of reduction along the liquid line of descent.

9. Conclusions

The Catface intrusions were emplaced at 40.4–41 Ma, contemporaneous with ore mineralization. The Catface porphyry Cu–Mo deposit is a reduced magmatic system based on ore mineralogy, apatite SO_3 contents, and fO_2 recorded by the assemblage K-feldspar–ilmenite–biotite–quartz. Intrusions at Catface were sill-like bodies of limited volume and emplaced at relatively shallow crustal depths of less than 4 km.

Magmas responsible for the generation of Catface were either derived from an inherently reduced source, or were reduced during ascent and emplacement. Both Sr and Nd isotopes from the Catface intrusives suggest a primitive source with no sedimentary assimilation and minimal crustal interaction. The geochemical affinity of the intrusions indicates a calc-alkaline, arc-related parent, which is typically oxidized. Parental magmas likely underwent reduction by loss of essentially all of its SO_2 by degassing, as evidenced by low S in apatite. The recognition of reduced, Paleogene, porphyry-generating magmatism on central Vancouver Island suggests consanguinity to other the Cascade Arc porphyry systems, such as North Fork, Washington.

Acknowledgments

We sincerely thank Jim Miller-Tait and Imperial Metals for their guidance and generous hospitality at the Catface deposit. We also thank M. Raudsepp for assistance with EMP analyses, and R. Creaser for carrying out the Re–Os age dating. The article benefited from reviews by J. Richards, M. Streck and editor A. Kerr. This research was supported by funding from Imperial Metals, the B.C. Ministry of Energy of Mines and NSERC of Canada.

Appendix A. Petrography of intrusive phases at Catface

Catface phase

The Catface phase is a medium-grained, medium to light gray, equigranular quartz diorite composed of: 40 to 60% subhedral 1–3 mm plagioclase grains with weak to moderate sericitization; 10–20% 1 to 2 millimeter quartz crystals with sutured 120° triple junction grain boundaries; 2–5% anhedral orthoclase with weak sericitization; 0.5–2 mm biotite as both primary grains (grains occur as single, larger, discrete crystals) with minor secondary clusters of much finer grains (0.5 to 1 mm). Alteration to chamosite varies from weak to pervasive in both primary and secondary phases. Anhedral amphibole (hornblende)

crystals 1 to 2 mm are often poikilitic with secondary biotite. Rare anhedral 0.5 to 1.5 millimeter clinozoisite and/or epidote crystals occur in late cross-cutting veinlets ($<5\%$ of the rock). Ilmenite is the dominant oxide, with trace magnetite. Apatite, zircon, and titanite are often included in primary biotites or plagioclase crystals.

Cliff/Halo phases

The Cliff and Halo phases are both medium-gray, porphyritic quartz diorite to granodiorite. The Halo phase contains “halos” of limonite around clusters of chalcopyrite and pyrite, distinguishing it from the Cliff phase. The phenocryst population is made up of 35–65% subhedral laths of hornblende ranging (0.5 to 2 mm) and 35 to 55% of sub-anhedral, 0.5 to 3 millimeter plagioclase laths with well-developed oscillatory zoning and strong sericitization. Rare anhedral 1 mm diameter phenocrysts of clinopyroxene are also observed. Chlorite commonly replaces amphiboles. The groundmass is composed of 55 to 60% plagioclase, 25 to 30% quartz, and approximately 10% amphibole. Accessory and/or opaque minerals include ilmenite, titanite, and disseminated secondary pyrite, chalcopyrite, pyrrhotite, \pm molybdenite, and \pm bornite.

Hornblende plagioclase porphyry (ADP) dykes

These dykes are a brownish purple rock with 20 to 30% phenocrysts ranging 1 to 3 millimeters in size, set in a fine-grained matrix. Phenocrysts are composed of 50 to 60% sub-to-anhedral plagioclase up to 3 millimeters in size, and 40 to 50% amphiboles, and/or their alteration products of biotite and chlorite (chamosite). The groundmass is composed of 60% plagioclase, 20% quartz, 10% biotite, and 10% amphibole. The fine-grained biotite and acicular actinolite exhibit moderate to strong chloritization. Opaque and accessory minerals include ilmenite, titanite, and secondary pyrite, chalcopyrite, \pm molybdenite, and \pm bornite.

Hecate Bay phase

The Hecate Bay phase is a fresh, medium-grained (1–3 mm), equigranular quartz diorite composed of 50–60% hornblende, 25–35% plagioclase, 5–10% quartz, and 2–5% potassium feldspar (microcline). Feldspars show oscillatory zoning, and quartz is typically interstitial and finer-grained. Rare epidote and clinozoisite are present as millimeter-scale veins ($<5\%$ of rock). Rare biotite is weakly altered to chlorite. Accessory zircon, apatite, ilmenite, and titanite occur throughout the rock, with trace magnetite, and secondary pyrite, chalcopyrite, and pyrrhotite.

Appendix B. Supplementary data

Supplementary data to this article can be found online at <http://dx.doi.org/10.1016/j.lithos.2012.08.001>.

References

- Ague, J.J., Brimhall, G.H., 1988. Magmatic arc asymmetry and distribution of anomalous plutonic belts in batholiths of California: effects of assimilation, crustal thickness, and depth of crystallization. *Geological Society of America Bulletin* 100, 912–927.
- Andersen, J.L., Lindsley, D.H., Davidson, P.M., 1993. QUILF—a Pascal program to assess equilibria among Fe–Mg–Mn–Ti oxides, pyroxenes, olivine, and quartz. *Computers and Geosciences* 19, 1333–1350.
- Anderson, J.L., 1996. Status of thermobarometry in granitic batholiths. *Transactions of the Royal Society of Edinburgh, Earth Science* 87, 125–138.
- Anderson, J.L., Smith, D.R., 1995. The effects of temperature and fO_2 on the Al-in-hornblende barometer. *American Mineralogist* 80, 549–559.
- Anderson, A.T., Wright, T.L., 1972. Phenocrysts and glass inclusions and their bearing on oxidation and mixing of basaltic magmas, Kilauea volcano, Hawaii. *American Mineralogist* 57, 188–216.
- Anderson, J.L., Barth, A.P., Wooden, J.L., Mazdab, F., 2008. Thermometers and thermobarometers in granitic systems. *Reviews in Mineralogy and Geochemistry* 69, 121–142.

- Andrew, A., Armstrong, R.L., Runkle, D., 1991. Neodymium–strontium–lead isotopic study of Vancouver Island igneous rocks. *Canadian Journal of Earth Sciences* 28, 1744–1752.
- Ballhaus, C., 1993. Redox states of lithospheric and asthenospheric upper mantle. *Contributions to Mineralogy and Petrology* 114, 331–348.
- Barnes, I., O'Neil, J.R., Trescases, J.J., 1978. Present day serpentinization in New Caledonia, Oman, and Yugoslavia. *Geochimica et Cosmochimica Acta* 42, 144–145.
- Bingen, B., Stein, H., 2003. Molybdenite Re–Os dating of biotite dehydration melting in the Rogaland high-temperature granulites, S Norway. *Earth and Planetary Science Letters* 208, 181–195.
- Brandon, M.T., 1989. Deformational styles in a sequence of olistostromal melanges, Pacific Rim Complex, western Vancouver Island, Canada. *Geological Society of America Bulletin* 101, 1520–1542.
- Buddington, A.F., Lindsley, D.H., 1964. Iron-titanium oxide minerals and synthetic equivalents. *Journal of Petrology* 5, 310–357.
- Burnham, C.W., Ohmoto, H., 1980. Late-stage processes of felsic magmatism. *Mining Geology, Special Issue* 8, 1–12.
- Burnham, C.W., Ohmoto, H., 1981. Late magmatic and hydrothermal processes in ore formation. *Mineral Resources: Genetic Understanding for Practical Applications*. National Academy Press, Washington, pp. 62–72.
- Candela, P.A., 1989. Felsic magmas, volatiles, and metallogenesis. *Society of Economic Geologists: Reviews in Economic Geology*, 4, pp. 223–233.
- Candela, P.A., 1997. A review of shallow, ore-related granites: textures, volatiles, and ore metals. *Journal of Petrology* 38, 1619–1633.
- Canil, D., Johnston, S.T., Laroque, J.P., Friedman, R., Heaman, L., in press. Age, construction and exhumation of intermediate mid-crust of the Jurassic Bonanza arc, Vancouver Island, Canada. *Lithosphere*.
- Carmichael, I.S.E., 1991. The redox states of basic and silicic magmas: a reflection of their source regions? *Contributions to Mineralogy and Petrology* 106, 129–141.
- Crowley, J.L., Schoene, B., Bowring, S.A., 2007. U–Pb dating of zircon in the Bishop Tuff at the millennial scale. *Geology* 35 (12), 1123–1126.
- Drummond, M.S., Defant, M.J., 1990. A model for trondhjemite–tonalite–dacite genesis and crustal growth via slab melting: Archean to modern comparisons. *Journal of Geophysical Research* 95 (B13), 21503–21521.
- Fairchild, L.H., Cowan, D.S., 1982. Structure, petrology, and tectonic history of the Leech River Complex northwest of Victoria, Vancouver Island. *Canadian Journal of Earth Sciences* 19, 1817–1835.
- Frost, B.R., 1985. On the stability of sulfides, oxides, and native metals in serpentinite. *Journal of Petrology* 26, 31–63.
- Frost, B.R., Beard, J.S., 2007. On silica activity and serpentinization. *Journal of Petrology* 48, 1351–1368.
- Frost, B.R., Barnes, C.G., Collins, W.J., Arculus, R.J., Ellis, D.J., Frost, C.D., 2001. A geochemical classification for granitic rocks. *Journal of Petrology* 42, 2033–2048.
- Gastil, G., Diamond, J., Knaack, C., Walawender, M., Marshall, M., Boyles, C., Chadwick, N., 1990. The problem of the magnetite/ilmenite boundary in southern and Baja California. *Geological Society of America Memoir* 174, 19–32.
- Green, T.H., Watson, E.B., 1979. Crystallization of apatite in natural magmas under high pressure, hydrous conditions, with particular reference to 'orogenic' rock series. *Contributions to Mineralogy and Petrology* 79, 96–105.
- Hammarstrom, J.M., Zen, E., 1986. Aluminum in hornblende: an empirical igneous geobarometer. *American Mineralogist* 71, 1297–1313.
- Holland, T.J.B., Blundy, J.D., 1994. Non-ideal interactions in calcic amphiboles and their bearing on amphibole–plagioclase thermometry. *Contributions to Mineralogy and Petrology* 116, 433–447.
- Holloway, J.R., 2004. Redox reactions in seafloor basalts: possible insights into silicic hydrothermal systems. *Chemical Geology* 210, 225–230.
- Hyndman, R.D., Peacock, S.M., 2003. Serpentinization of the forearc mantle. *Earth and Planetary Science Letters* 212, 417–432.
- Imai, A., 2002. Metallogenesis of porphyry Cu Deposits of the western Luzon Arc, Philippines: K–Ar ages, SO₃ contents of microphenocrystic apatite and significance of intrusive rocks. *Resource Geology* 52, 147–161.
- Imai, A., 2004. Variation of Cl and SO₃ contents of microphenocrystic apatite in intermediate to silicic igneous rocks of Cenozoic Japanese Island Arcs: implications for porphyry Cu Metallogenesis in the Western Pacific Island Arcs. *Resource Geology* 54, 357–372.
- Isachsen, C.E., 1987. Geology, geochemistry, and cooling history of the Westcoast Crystalline Complex and related rocks, Meares Island and vicinity, Vancouver Island, British Columbia. *Canadian Journal of Earth Sciences* 24, 2047–2064.
- Ishihara, S., 1977. The magnetite-series and ilmenite-series granitic rocks. *Mining Geology* 27, 293–305.
- Ishihara, S., 1981. The granitoid series and mineralization. *Economic Geology*, 75th Anniversary, pp. 458–484.
- Jaffey, A.H., Flynn, K.F., Glendenin, L.E., Bentley, W.C., Essling, A.M., 1971. Precision measurement of half-lives and specific activities of ²³⁵U and ²³⁸U. *Physical Review C: Nuclear Physics* 4, 1889–1906.
- Johnson, M.E., Rutherford, M.J., 1989. Experimental calibration of the aluminum-in-hornblende geobarometer with application to Long Valley caldera (California). *Geology* 17, 837–841.
- Kelley, K.A., Cottrell, E., 2012. The influence of magmatic differentiation on the oxidation state of Fe in a basaltic arc magma. *Earth and Planetary Science Letters* 329–330, 109–121.
- Leake, B.E., Woolley, A.R., Arps, C.E.S., Birch, W.D., Gilbert, M.C., Grice, J.D., Hawthorne, F.C., Kato, A., Kisch, H.J., Krivovichev, V.G., Linthout, K., Laird, J., Mandarino, J.A., Maresch, W.V., Nickel, E.H., Rock, N.M.S., Schumacher, J.C., Smith, D.C., Stephenson, N.C.N., Ungaretti, L., Whittaker, E.J.W., Youzhi, G., 1997. Nomenclature of amphiboles: report of the subcommittee on amphiboles of the International Mineralogical Association, Commission on New Minerals and Mineral Names. *American Mineralogist* 82, 1019–1037.
- Lee, C.A., Leeman, W.P., Canil, D., Li, Z.A., 2005. Similar V/Sc systematics of MORB and arc basalts: implications for the oxygen fugacities of their mantle source regions. *Journal of Petrology* 46, 2313–2336.
- Madsen, J., 2004. Geochemistry and geochronology of Eocene forearc magmatism on Vancouver Island: implications for Cenozoic to recent plate configurations in the Pacific basin. Masters Thesis, Simon Fraser University.
- Madsen, J., Thorkelson, J., Friedman, R., Marshall, D., 2006. Cenozoic to recent plate configurations in the Pacific Basin: ridge subduction and slab window magmatism in western North America. *Geosphere* 2, 11–34.
- Mathez, E.A., 1984. Influence of degassing on oxidation states of basaltic magmas. *Nature* 310, 371–375.
- Mattinson, J.M., 2005. Zircon U–Pb chemical abrasion (“CA-TIMS”) method: combined annealing and multi-step partial dissolution analysis for improved precision and accuracy of zircon ages. *Chemical Geology* 220, 47–66.
- McDonough, W.F., Sun, S.S., 1995. The composition of the earth. *Chemical Geology* 120, 223–253.
- McDougall, J.J., 1976. Catface Porphyry Deposits of the Canadian Cordillera, Part B – Porphyry Copper and Copper–Molybdenum Deposits of the Calc-Alkaline Suite – Special Volume 15, Paper 29, pp. 299–310.
- McDougall, J.J., Enns, S.G., 1995. Catface Copper Molybdenum Porphyry, West Central Vancouver Island, British Columbia: An Update. *Porphyry Deposits of the Northwestern Cordillera of North America: The Canadian Institute of Mining and Metallurgy, Special*, 46, pp. 322–326.
- Middlemost, A.K., 1994. Naming materials in the magma/igneous rock system. *Earth-Science Reviews* 37, 215–224.
- Miyashiro, A., 1974. Volcanic rocks series in island arcs and active continental margins. *American Journal of Science* 274, 321–355.
- Moody, J.B., 1976. Serpentinization: a review. *Lithos* 9, 125–138.
- Mueller, R.F., 1971. Oxidative capacity of magmatic components. *American Journal of Science* 270, 236–243.
- Muller, J.E., Carson, D.J., 1969. Geology and mineral deposits of Alberni map-area, British Columbia (92 F). *Geological Survey of Canada, Paper* 68–50.
- Mundil, R., Ludwig, K.R., Metcalfe, I., Renne, P.R., 2004. Age and timing of the Permian mass extinctions: U/Pb dating of closed-system zircons. *Science* 305, 1760–1763.
- Mustard, P., 1994. The Upper Cretaceous Nanaimo Group, Georgian Basin. In *Geology and Geological Hazards of the Vancouver Region*. Geological Survey of Canada Bulletin 481, 27–95.
- Ohmoto, H., Goldhaber, M.B., 1997. Sulfur and carbon isotopes. In: Barnes, H.L. (Ed.), *Geochemistry of Hydrothermal Ore Deposits*. John Wiley & Sons, New York, pp. 517–611.
- Parat, F., Holtz, F., 2004. Sulfur partitioning between apatite and melt and effect of sulfur on apatite solubility at oxidizing conditions. *Contributions to Mineralogy and Petrology* 247, 201–212.
- Parat, F., Dungan, M.A., Streck, M.J., 2002. Anhydrite, pyrrhotite, and sulphur-rich apatite: tracing the sulphur evolution of an Oligocene andesite (Eagle Mountain, CO, USA). *Lithos* 64, 63–75.
- Peng, G., Luhn, J.F., McGee, J.J., 1997. Factors controlling sulphur concentrations in apatite. *American Mineralogist* 82, 1210–1224.
- Pivinskii, A.J., 1968. Experimental studies of igneous rock series: Central Sierra Nevada batholiths, California. *Journal of Geology* 76, 548–570.
- Raith, J.G., Stein, H.J., 2000. Re–Os dating and sulfur isotope composition of molybdenite from tungsten deposits in western Namaqualand, South Africa: implications for ore genesis and the timing of metamorphism. *Mineralium Deposita* 35, 741–753.
- Richards, J.P., 1990. Petrology and geochemistry of alkalic intrusives at the Porgera gold deposit, Papua New Guinea. *Journal of Geochemical Exploration* 35, 141–199.
- Rowins, S.M., 2000. Reduced porphyry copper–gold deposits: a new variation on an old theme. *Geology* 28, 491–494.
- Scaillet, B., MacDonald, R., 2006. Experimental and thermodynamic constraints on the sulphur yield of peralkaline and metaluminous silicic flood eruptions. *Journal of Petrology* 47, 1413–1437.
- Scaillet, B., Clemente, B., Evans, B.W., Pichavant, M., 1998. Redox control of sulfur degassing in silicic magmas. *Journal of Geophysical Research* 103 (B10), 23,937–23,949.
- Schmidt, M.W., 1992. Amphibole composition in tonalite as a function of pressure: an experimental calibration of the Al-in-hornblende barometer. *Contributions to Mineralogy and Petrology* 110, 304–310.
- Schmidt, M.W., Thompson, A.B., 1996. Epidote in calcalkaline magmas: an experimental study of stability, phase relationships and the role of epidote in magmatic evolution. *American Mineralogist* 81, 462–474.
- Schmitz, M.D., Schoene, B., 2007. Derivation of isotope ratios, errors, and error correlations for U–Pb geochronology using ²⁰⁵Pb–²³⁵U–(²³³U)–spiked isotope dilution thermal ionization mass spectrometric data. *Geochemistry, Geophysics, Geosystems* 8, Q08006 <http://dx.doi.org/10.1029/2006GC001492>.
- Scoates, J.S., Friedman, R.M., 2008. Precise age of the platinumiferous Merensky Reef, Bushveld Complex, South Africa, by the U–Pb zircon chemical abrasion ID-TIMS technique. *Economic Geology* 103, 465–471.
- Seedorf, E., Dilles, J.H., Proffett, J.M., Einaudi, M.T., Zurcher, L., Stavast, W.J.A., Johnson, D.A., Barton, M.D., 2005. Porphyry deposits: characteristics and origin of hypogene features. 100th Anniversary of Economic Geology, pp. 251–298.
- Selby, D., Creaser, R.A., 2001. Late and mid-Cretaceous mineralization in the northern Canadian Cordillera: constraints from Re–Os molybdenite dates. *Economic Geology* 96, 1461–1467.
- Simpson, R.G., Chapman, J., 2009. Mineral Resource Estimate, Catface Copper, Internal Report. GeoSim Services Inc., Vancouver, Canada.

- Sinclair, W.D., 2007. Porphyry deposits. *Mineral Deposits of Canada, A Synthesis of Major Deposit Types, District Metallogeny, the Evolution of Geological Provinces, and Exploration Methods*: Geological Association of Canada, Mineral Deposits Division, Special Publication No. 5, pp. 223–244.
- Smithson, D.M., 2004. Late Eocene tectono-magmatic evolution and genesis of reduced porphyry copper–gold mineralization at the North Fork deposit, Central Cascades Mountain Range, Washington, U.S.A. Master's Thesis, University of British Columbia.
- Stacey, J.S., Kramers, J.D., 1975. Approximation of Terrestrial Lead Isotope Evolution by a 2-Stage Model. *Earth and Planetary Science Letters* 26 (2), 207–221.
- Stein, H.J., Markeya, R., Hannah, J.L., Zimmerman, A., Selby, D., Creaser, R.A., 2007. Standardizing Re–Os geochronology: a new molybdenite reference material (Henderson, USA) and the stoichiometry of Os salts. *Chemical Geology* 244, 74–87.
- Streck, M., Dilles, J.H., 1998. Sulfur evolution of oxidized arc magmas as recorded in apatite from a porphyry copper batholith. *Geology* 26, 523–526.
- Takagi, T., 2004. Origin of magnetite- and ilmenite-series granitic rocks in the Japan Arc. *American Journal of Science* 304, 169–202.
- Wones, D.R., 1989. Significance of the assemblage titanite + magnetite + quartz in granitic rocks. *American Mineralogist* 74, 744–749.
- Wones, D.R., Eugster, H.P., 1964. Stability of biotite: experiment, theory, and application. *American Mineralogist* 50, 1228–1271.
- Zajacz, Z., Candela, P.A., Piccoli, P.M., Sanchez-Valle, C., 2012. The partitioning of sulfur and chlorine between andesite melts and magmatic volatiles and the exchange coefficients of major cations. *Geochimica et Cosmochimica Acta* 89, 81–101.